Wind waves in shallow microtidal basins and the dynamic equilibrium of tidal flats

S. Fagherazzi,[1] C. Palermo,[2] M. C. Rulli,[2] L. Carniello,[3] and A. Defina[3]

[1]   Shallow microtidal basins are characterized by extensive areas of tidal flats that lie within specific ranges of elevation. These landforms are inherently flat and their evolution strongly depends on the balance between sedimentary and erosive processes. Here we present a stochastic point model for tidal flat evolution to study the influence of tidal currents and wind waves on tidal flat equilibrium. The model accounts for sediment deposition and sediment resuspension by wind waves and is applied to the Venice lagoon, Italy. Model results show that the equilibrium elevation of tidal flats depends on the relationship between shear stress caused by wind waves and depth. It is found that wind wave shear stresses peak for a specific water depth which is a function of the local wave climate and fetch distance. Above this critical depth, tidal flats are unstable, since an increase in elevation reduces wave height and therefore erosion, preventing the system from recovering equilibrium conditions. The critical depth for equilibrium depends on fetch distance but not on substrate characteristics and, for the Venice lagoon, varies from −1.5 m for unlimited fetch (>3000 m) to −0.6 m for a fetch of 1000 m. The sediment characteristics determine instead the sediment input necessary to maintain the tidal flat in equilibrium at a specific elevation. Sediment inputs for tidal flats composed of fine sand need to be much higher than those required for tidal flats composed of cohesive material. Finally, we show that the spring-neap modulation of the tide is critical for tidal flat equilibrium, with erosive events occurring mostly during spring conditions that equilibrate the sediment deposition during neap tide.

1. Introduction

[2]   Shallow microtidal basins are characterized by extensive areas of tidal flats and salt marshes that lie within specific ranges of elevation. Both landforms are inherently flat, and their evolution strongly depends on the balance between sedimentary and erosive processes. Specifically, salt marsh elevation is controlled by mineral and organogenic sediment accumulation [*Pethick*, 1981], sea level variations, and by the stabilizing effect of halophyte vegetation on its platform [*Morris et al.*, 2002; *Mudd et al.*, 2004; *Silvestri et al.*, 2005], whereas tidal flats stem from a delicate balance between sediment deposition and resuspension by wind waves and tidal currents [*Allen and Duffy*, 1998]. Bathymetric data show that the intertidal landscape in shallow basins is organized in a bimodal distribution of elevations, with the two peaks corresponding to salt marshes and tidal flats and few areas lying at intermediate

elevations [*Fagherazzi et al.*, 2006]. A recently developed conceptual model indicates that this bimodal distribution of elevations is the effect of a decrease in wind wave shear stresses in shallow waters [*Fagherazzi et al.*, 2006].

[3]   Here we present a stochastic point model for tidal flat evolution that explores the validity and limits of the hypothesis by *Fagherazzi et al.* [2006]. Point models have been already utilized for studying the evolution of salt marshes. In the pioneering work of *Krone* [1987], changes in marsh elevation are calculated as a function of sediment concentration, settling velocity of the suspended sediment flocs, and hydroperiod. When the marsh platform becomes emergent, the inundation period decreases, so that less sediment deposits leading to a reduction of marsh accretion. The model was then improved by considering sediment supply and sea level rise [*Allen*, 1990; *French*, 1993], sediment composition [*Allen*, 1995], differences in sedimentation rates between creek levees and marsh platform [*Temmerman et al.*, 2004a], and variations in sediment concentration as a function of tidal inundation [*Temmerman et al.*, 2004b]. In recent years, a major development has been the inclusion in the marsh model of the vegetation effects on sediment dynamics, accumulation rates, and organogenic production by linking all these processes to the biomass of halophyte vegetation that colonizes the

[1]Department of Earth Sciences and Center for Computational Science, Boston University, Boston, Massachusetts, USA.
[2]Department of Hydraulic, Environmental, Road and Surveying Engineering Hydraulics, Politecnico di Milano, Milan, Italy.
[3]Department IMAGE, University of Padova Via Loredan, Padua, Italy.

marsh surface [*Morris et al.*, 2002; *Mudd et al.*, 2004, *D'Alpaos et al.*, 2006].

[4] However, none of these models focuses on the evolution of tidal flats and the incipient formation of salt marshes. As a consequence, point models of salt marsh evolution can only be applied to locations in which the salt marsh is already present but are ineffective in determining under what conditions the salt marsh has evolved from tidal flats. From this scientific perspective, the point model of tidal flat evolution in the work of *Cappucci et al.* [2004] is the first to correctly represent all the processes at play in these environments. Specifically, *Cappucci et al.* [2004] include in their model tidal currents and wind waves and their effect on the erosion of bottom sediments and deposition of suspended sediments. Here we extend the framework of *Cappucci et al.* [2004] to the long-term dynamics of tidal flats and determine a key characteristic of the system, the conditions required for transition from tidal flats to salt marshes.

[5] To this end, we develop a stochastic point model for tidal flat evolution, and we apply it to the Venice lagoon, Italy, which is a microtidal basin (tidal range of 0.7 m) that has experienced large sediment loss during the last century [*Fagherazzi et al.*, 1999; *Rinaldo et al.*, 1999a, 1999b; *Marani et al.*, 2003; *Fagherazzi et al.*, 2006].

2. Critical Bifurcation of Microtidal Landforms

[6] Following the conceptual model by *Fagherazzi et al.* [2006] for a prescribed, geomorphically significant wind intensity, we can plot the total shear stress (sum of the waves and tidal currents shear stresses) as a function of tidal flat elevation in a microtidal basin. The bottom shear stress, after reaching a maximum, decreases in shallow water where dissipative processes (bottom friction, wave breaking, and whitecapping) limit the maximum height of the wind waves (Figure 1). This maximum of shear stress bears important consequences for the morphological transition from tidal flats to salt marshes and for the overall redistribution of sediments in shallow coastal basins. *Fagherazzi et al.* [2006] assume an average annual sedimentation rate that is site dependent but constant during bottom evolution and suppose that the sediment resuspended on tidal flats during a storm is directly proportional to the difference between bottom shear stress and the critical shear stress for sediment erosion.

[7] We begin our analysis from a tidal flat with an elevation below mean sea level. At the initial stages of the evolution, the water depth is so high that the wave-induced bottom shear stress is smaller than the critical shear stress for erosion, so that the bottom elevation increases in time because of deposition (Figure 1a, right side). At a certain point, the bottom elevation is high enough so that the waves start resuspending bottom sediments. Following this transition, we subtract the average annual erosion from the average annual deposition (see Figure 1a) at every time step. Since the erosion rate is proportional to the difference between shear stress and the critical shear stress, then the average annual erosion is proportional to the distance between the solid line (wave shear stress) and the dotted line (critical shear stress) in Figure 1a. If the annual deposition is smaller than the maximum erosion, the tidal
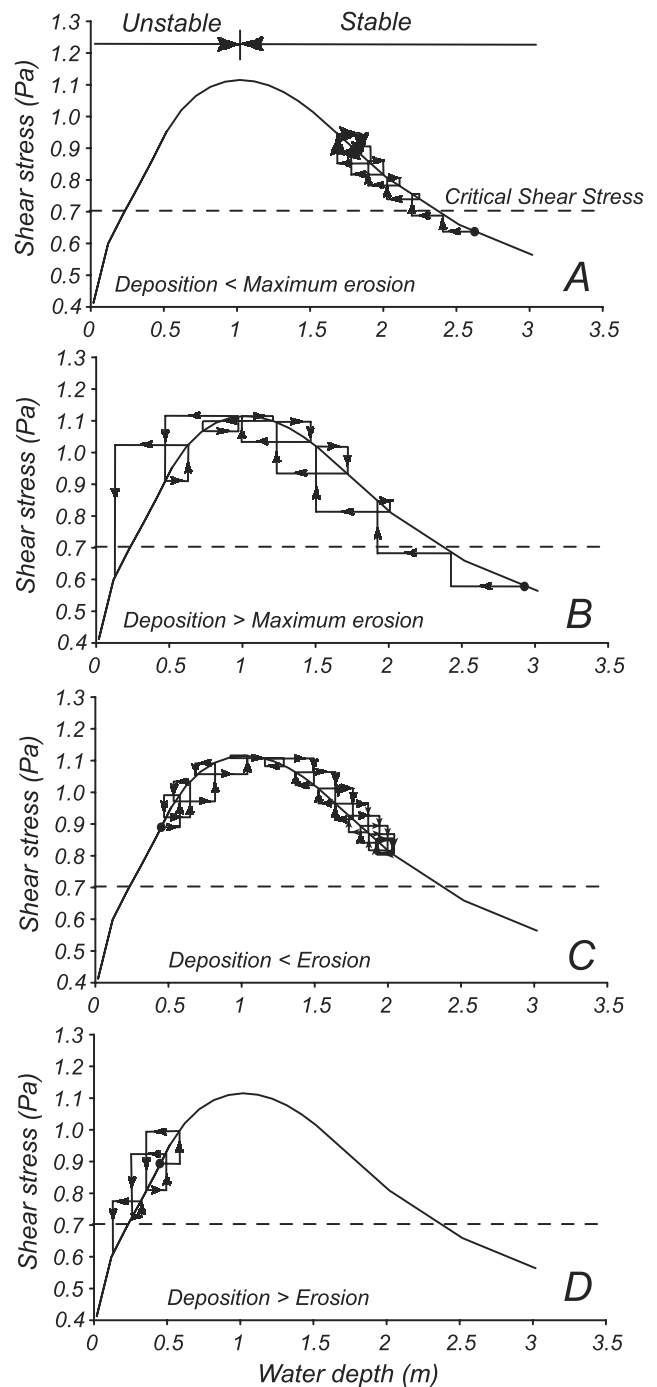

Figure 1. Morphological evolution of tidal flats as a function of bottom shear stresses produced by wind waves. The trajectories are based on the assumption of constant annual deposition and specified wind speed and duration. Trajectory of bottom elevation for a point starting in the stable branch of the curve, (a) deposition lower than peak erosion, (b) deposition higher than peak erosion. Trajectory of bottom elevation for a point starting in the unstable branch of the curve, (c) deposition lower than erosion, (d) deposition higher than erosion. The shear stress curve has been calculated for a characteristic wind speed of 8 m/s and assuming an average tidal current velocity of 0.16 m/s, the typical value for tidal flats in the Venice lagoon, Italy.
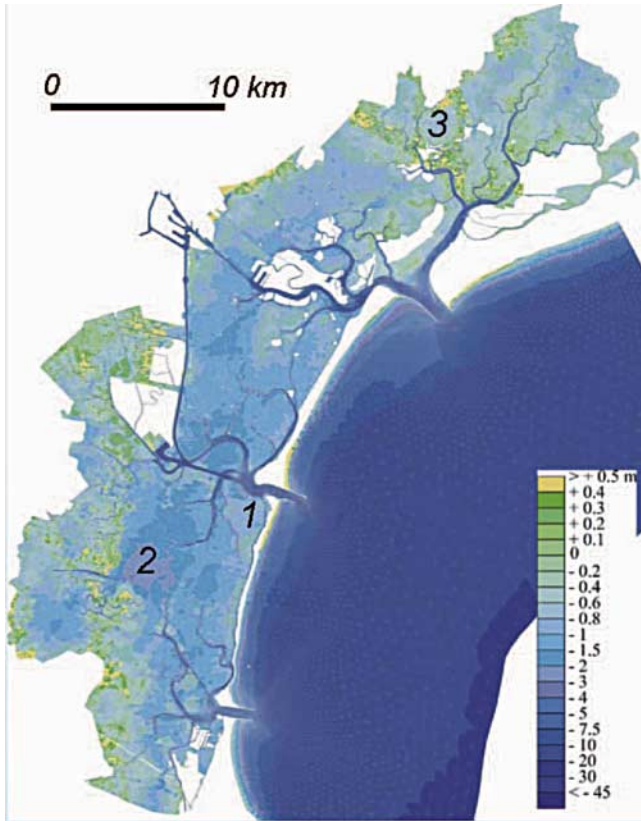
Figure 2. Bathymetry of the Venice lagoon, Italy, and location of the three tidal flats used in the simulations.

flat inevitably evolves to a position on the curve in Figure 1a where the average annual deposition balances the average annual erosion, and the bottom elevation is in dynamic equilibrium (bold square in Figure 1a). We refer to the branch of the curve from the peak to the right as morphologically stable, since deposition is counteracted by an increase in erosion because of higher shear stresses at the bottom. In this part of the curve, the tidal flat adjusts its elevation to a position of dynamic equilibrium that depends on deposition rate and wave erosion.

[8] If the annual deposition is greater than the maximum erosion, then the vertical accretion of the tidal flat passes the peak and any further increase in elevation leads to smaller bottom shear stresses. Less erosion produces a marked increase in elevation, in a self-reinforced process that eventually gives form to an emergent salt marsh (see Figure 1b). Once the elevation becomes higher than mean sea level, the accretion dynamics is marginally affected by waves. The main factors that determine the final marsh elevation are sediment supply, organic production driven by vegetation encroachment, and sediment compaction. The marsh is stable up to large fluctuations in relative sea level and storm intensity, so that it can be considered a resting point of our dynamics. The left branch of the curve is morphologically unstable because an increase in deposition beyond the maximum induces a fast vertical accretion. All the elevations lower than the peak are unlikely to maintain a stable tidal flat, since the processes at play tend to fill up the area and create a salt marsh. The unstable character of the left branch is even more evident if we consider as initial

condition a point on this part of the curve (Figure 1c and 1d). The initial configuration could persist only if the local deposition rate exactly balances the erosion rate, otherwise the bottom elevation will evolve toward either a stable tidal flat, if the annual deposition rate is smaller than the local erosion rate (Figure 1c), or emergent salt marsh, if the annual deposition rate is higher than the erosion rate (Figure 1d).

[9] The conceptual model presented in Figure 1 is expanded in this research by including the variability of wind conditions and tides in the Venice lagoon (Figure 2). We will also investigate the role of sediment characteristics and fetch distance on the dynamic equilibrium of tidal flats and their evolution in time.

3. Tidal Currents and Wind Waves Bottom Shear Stresses

[10] In microtidal environments, the resuspension of bottom sediments in areas far from the inlets and tidal channels is mostly due to wind waves during storm activity [*Carniello et al.*, 2005]. However, tidal oscillations of the water surface in the basin produce fluxes that enhance bottom shear stresses, favoring sediment erosion and transport. Tidal currents are a function of the basin geometry, bathymetry, and the presence of nearby tidal channels. In general, the current velocity is negligible at high and low tide (slack water) and maximum in proximity of mean sea level, when the variation in water elevation per unit time is maximum.

[11] The total bottom shear stress, responsible for sediment resuspension, is a nonlinear combination of the wave shear stress and the tidal current shear stress [*Soulsby*, 1997]:

$$4\tau_{tot} = \tau_{wave} + \tau_{curr}\left[1 + 1.2\left(\frac{\tau_{wave}}{\tau_{curr} + \tau_{wave}}\right)^{3.2}\right] \quad (1)$$

where τ_{wave} is the shear stress produced by wind waves, and τ_{curr} is the shear stress caused by tidal currents. In this paragraph, we outline the procedure to obtain both values in time.

[12] Tidal oscillations in the Venice lagoon are reproduced by using the eight principal harmonics of the astronomic signal [see *Rinaldo et al.*, 1999b]. In a simplified framework, we can link the tidal velocity to the first derivative of the water level [*Fagherazzi et al.*, 2003]:

$$u_0 = u_{\max}\frac{\dfrac{d\eta(t-\phi)}{dt}}{\dfrac{d\eta}{dt}\big|_{\max}} \quad (2)$$

where η is the water level, Φ is the phase difference between water level and velocity peak, and $u_{\max}$ is a constant that varies within the lagoon and determines the maximum velocity at that particular location. $u_{\max}$ and Φ are determined by fitting equation (2) to the results of a fully two-dimensional shallow water model for the Venice lagoon [*Carniello et al.*, 2005]. In Figure 3, we report a comparison between the velocity calculated by the shallow water model and the approximation (2) at location 1 (Figure 2). The
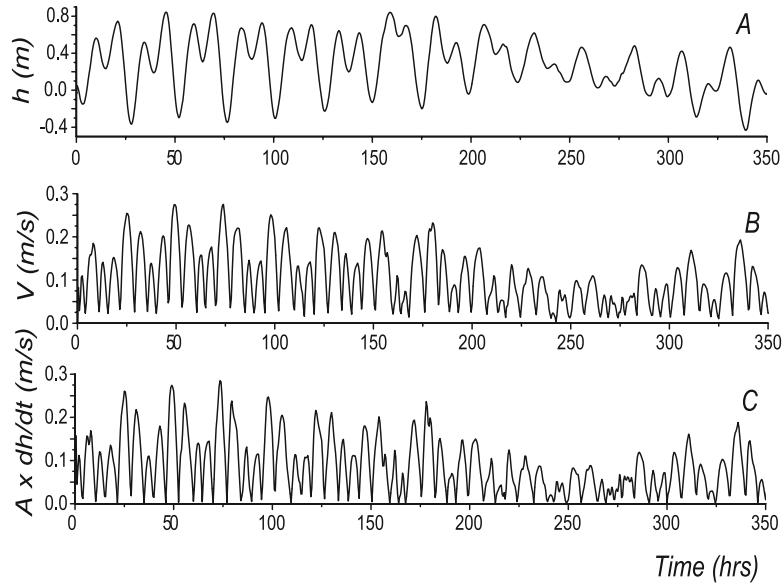
Figure 3. Comparison between tidal velocities and changes in water level for location 1 in Figure 2. The water surface elevation and the velocity were calculated with a two-dimensional finite element model. (a) Surface elevation, (b) tidal velocity, (c) derivative of the water surface. The derivative of the water surface is shifted of 30 min.

velocities are highly correlated ($R = 0.91$), and the pattern is very well reproduced by the simplified model. Similar results also apply for locations 2 and 3 ($R = 0.90$ and $R = 0.59$, respectively). The maximum tidal velocity and the phase difference Φ are reported in Table 1.

[13] During tidal flat evolution, it is reasonable to assume that tidal velocities will vary as a result of the overall morphological changes of the basin (shoaling, deepening, and lateral extension). Clearly a description of the morphological evolution of the entire Venice lagoon is beyond the scope of this study, but we can still derive a generic trend by plotting maximum tidal velocity as a function of tidal elevation for every tidal flat in the lagoon. The tidal velocity is computed with the two-dimensional finite elements model presented in the work of *Carniello et al.* [2005] for a spring tide (Figure 4).

[14] Despite the substantial scatter in the data, an average trend of reduction in tidal velocity with shallow depths emerges from the analysis. For depths higher than 2.5 m, the peak velocity flattens out or slightly decreases. By assuming that the ergotic principle is valid in this environment, and that therefore the distribution of tidal flat elevation in space represents all the possible evolutive stages of the system in time [see also *Gardner*, 2004], we can then apply the trend

described in Figure 4 (i.e., a decrease of tidal velocity with elevation) to our three sites during evolution.

[15] We then assume that the maximum tidal velocity decreases by two thirds when the tidal flat evolves from a depth of 2.5 m to mean sea level. The new tidal velocity is then:

$$u = u_0 \left(\frac{1}{3} + \frac{2}{3} \frac{h}{h_{ref}} \right) \qquad (3)$$

where h_{ref} is the reference depth of 2.5 m, and u_0 is the velocity at a depth of 2.5 m.

[16] The corresponding shear stress is:

$$\tau_{curr} = C_f \rho u^2 \qquad (4)$$

where C_f is a friction coefficient assumed herein to be 0.01, and ρ is the water density. Wind waves are generated by the transfer of energy from the wind to the water surface. Starting from a flat water surface, the wind generates waves that increase in height until the energy dissipation produced by different processes limits the wave growth. White-capping and depth-induced breaking reduce the maximum wave height for a given water depth, while bottom friction

Table 1. Sediment and Hydrodynamic Characteristics of Three Tidal Flats in the Venice Lagoon the Locations are Reported in Figure 2

	D_{50}, μm	h, m	τ_{cr}, Pa	ρ^b, kg/m^3	Settling Velocity	Max Tidal Velocity, m/s	Phase Delay, hrs	Fetch, m	Erosion Coefficients
1	74[a]	−2.0	0.65[a]	1850[a]	W_s= 0.005 m/s	0.30[b]	1[b]	>3000	$\alpha = 4.12 \times 10^{-4}$[c]
2	22[a]	−2.5	0.84[a]	1750[a]	$K = 0.00077^a$ m^5/s/kg$^{4/3}$	0.25[b]	1[b]	>3000	$\beta = 4.12 \times 10^{-4}$[c] $\gamma = 0.0054$[d]
3	23[a]	−0.6	0.57[a]	1650[a]	$K = 0.00077^a$ m^5/s/kg$^{4/3}$	0.31[b]	0.5[b]	1000	$\beta = 4.12 \times 10^{-4}$[c] $\gamma = 0.0054$[d]

[a]From the field survey of *Amos et al.* [2004].
[b]From numerical simulations with the model presented in *Carniello et al.* [2005].
[c]From *Capucci et al.* [2004].
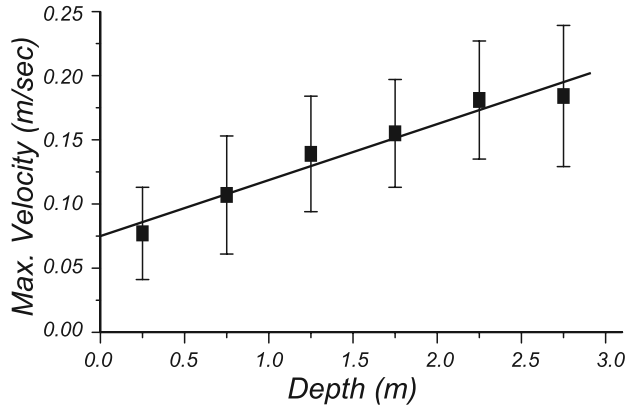[d]From *Sanford and Maa* [2001].

Figure 4. Maximum tidal velocity as a function of water depth. The velocity was computed with a two-dimensional finite elements model that solves the shallow water equations. The velocities of 8973 tidal flat elements were then binned every 0.5 m of elevation.

further enhances wave decay by intense energy dissipation. An equilibrium is reached when the energy generated by the wind action equals the total energy dissipated by bottom friction, whitecapping, and breaking. In this situation, the sea is fully developed, and the height of the wave is the maximum possible for that particular bathymetry. More importantly, this condition develops the highest bottom shear stresses, which ultimately lead to bottom sediment erosion. The equilibrium condition can be expressed as:

$$E_w = E_{bf} + E_{wc} + E_b \qquad (5)$$

where E_w is the wave energy generated by the wind, E_{bf}, E_{wc}, and E_b are the energy dissipation because of bottom friction, whitecapping, and breaking, respectively.

[17] Following *Booij et al.* [1999] and *Carniello et al.* [2005], all these terms can be expressed as a function of wave energy, so that equation (5) becomes:

$$\alpha + \beta E = 2C_f \frac{k}{\sinh(2kh)}E + c\sigma\left(\frac{\gamma}{\gamma_{PM}}\right)^m E + \frac{2a}{T}Q_b\left(\frac{H_{\max}}{H}\right)^2 E \qquad (6)$$

where $E = \rho_w g H^2 / 8$ is the wave energy, H, T, and k are the wave height, period, and wave number, respectively, h is the water depth, and the parameters α and β depend on the wind velocity U_w. The values of all the other parameters utilized to solve equation (6) are reported in the work of *Fagherazzi et al.* [2006] and in the work of *Carniello et al.* [2005].

[18] The solution of equation (6) determines the wave height as a function of the wind speed and water depth. Once the wave height is known, we can derive the bottom shear stresses from the expressions:

$$\tau_b = \frac{1}{2}f_w\rho_w u_m^2 \qquad \text{with} \qquad u_m = \frac{\pi H}{T\sinh(kh)} \qquad (7)$$

where f_w is a friction factor, and u_m is the maximum horizontal orbital velocity at the bottom associated with the wave. u_m directly depends on wave height H and water

depth h so that higher waves produce larger bottom shear stresses. The wave model was successfully tested against waves measured in the Venice lagoon in the work of *Carniello et al.* [2005].

[19] So far, we have considered only fully developed conditions, in which the wind blows over a distance (fetch) long enough to allow the maximum transfer of energy to the water surface.

[20] When the wind is obstructed by islands and salt marshes, the transfer of energy to the ocean surface is not complete and smaller waves form. In order to calculate the fetch influence on wave height, we solve the full equation for the propagation of wave action [see *Booij et al.*, 1999; *Carniello et al.*, 2005]:

$$\frac{\partial N}{\partial t} + C_g \cdot \nabla N = \frac{1}{\sigma}\left(E_w - E_{bf} + E_{wc} + E_b\right) \qquad (8)$$

where N is the wave action (energy divided by wave frequency σ and $C_g = (C_{gx}, C_{gy})$ is the wave group celerity. For any depth, equation 8 is solved along a transect of length equal to the fetch. The shear stress corresponding to the maximum wave height is then plotted in Figure 5.

4. Wind Intensity and Duration

[21] In order to simulate the evolution of tidal flat elevation in a basin, we need to reproduce the wind characteristics (intensity, duration, and frequency) in time. To this end, we use a Montecarlo approach based on long-term wind data for the Venice lagoon. To reproduce wind intensities, we use 26 years of wind statistics in the Venice lagoon, whereas for the wind duration, we use high-resolution measurements collected every 15 min from October 2002 to March 2003.

[22] The wind intensity data were binned in six intervals of 2.5 m/s of amplitude, ranging from 0 to 15 m/s. By interpolating the velocity against the logarithm of the frequency, we obtain the equation (Figure 6, with $R = 0.99$):

$$U = -5.62 * \ln f + 0.747 \qquad (9)$$

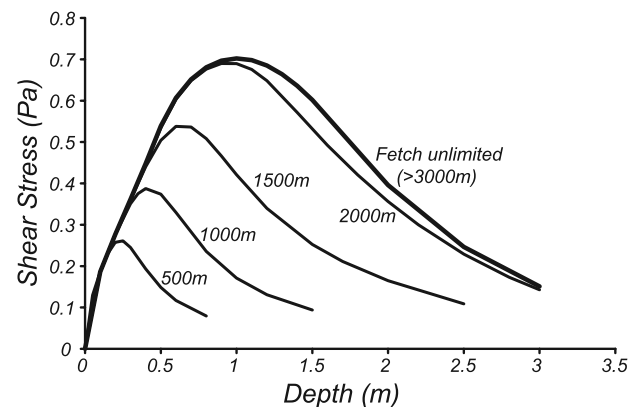where U is the wind speed (m/s), and f is the relative frequency of a wind with intensity U.

Figure 5. Distribution of shear stress as a function of water depth for different fetch lengths.
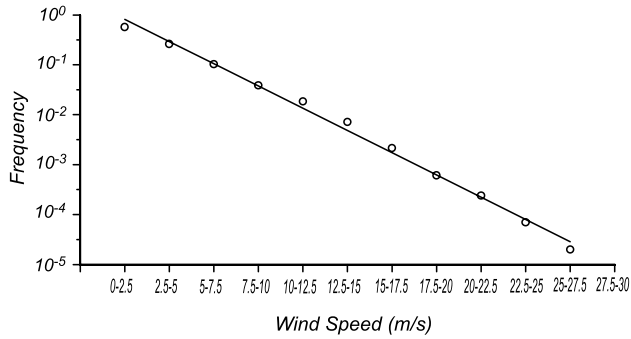
Figure 6. Frequency of wind speed in the Venice lagoon during the period 1951–1977.

[23] For each wind speed class, we then study the corresponding wind duration from October 2002 to March 2003 in a log-log plot.

[24] The interpolation of frequency against duration is reported in Figure 7. We notice that the duration is relatively independent of the speed, so that we can assume, for sake of simplicity, a unique distribution of durations for all intensities:

$$D_{wind} \cong 690 \times f^{-0.65} \qquad (10)$$

where D is the duration (s) and f the frequency.

[25] Only for high wind speeds, the duration departs from equation 10, but the reduced number of data cannot provide a significant estimate for these extreme events. Since we want to randomly sample the wind speed U and the duration D according to the probability distributions (9) and (10), we resort to the inverse transform method, after normalizing the distributions and calculating the corresponding cumulative distributions. We thus obtain the expressions:

$$U = -5.62 \ln\left(\frac{1.0118 - r}{1.579}\right) \qquad \text{and}$$
$$D_{wind} = \left(\frac{1.0975 - r}{42.64}\right)^{-1.86} \qquad (11)$$

for the wind speed (m/s) and duration (s), respectively, where r is a random number uniformly distributed between 0 and 1.

5. Point Model of Tidal Flat Bottom Evolution

[26] Once the shear stresses of the tidal currents and wind waves are calculated, we can study the variations of tidal flat elevation in time with a point model of tidal flat bottom evolution. In our approach, we consider a point in a tidal flat and analyze its evolution in time by applying the mass balance [*Exner*, 1925] equation:

$$\rho_b \frac{dz_b}{dt} = D - E \qquad (12)$$

where ρ_b is the sediment density measured in the field (see Table 1 and *Amos et al.* [2004]), z_b is bottom elevation, D is the deposition rate, and E is the erosion rate.

[27] The deposition rate at each point in the basin depends on the local availability of suspended sediment,

on the sediment input from rivers debouching into the lagoon, on the net export of sediments to the ocean, and, more generally, on the characteristics of sediment transport in the nearshore area.

[28] The sediment concentration in the water column depends on the material eroded or deposited at the bottom as well as on the lateral exchanges of sediment. We can then write:

$$\frac{\partial(hC)}{\partial t} + \nabla(uhC) = E - D \qquad (13)$$

where C is the concentration of suspended sediment, and h is the water depth. Since the characterization of the spatial patterns of sediment deposition is beyond the scope of this analysis, we adopt a simplified framework for the divergence of the sediment flux in equation (13) that highlights the dependence of the sediment input on tidal velocity as well as the dependence of the sediment output on the local value of concentration.

[29] The divergence of sediment flux per unit area of tidal flat is averaged and simplified as:

$$\nabla(uhC) = \frac{u}{u_{max}}\left(M - \frac{f}{T}Ch\right) \qquad (14)$$

where M is the maximum sediment input per unit area (kg/s/m²) during a spring tide, and it is redistributed in the
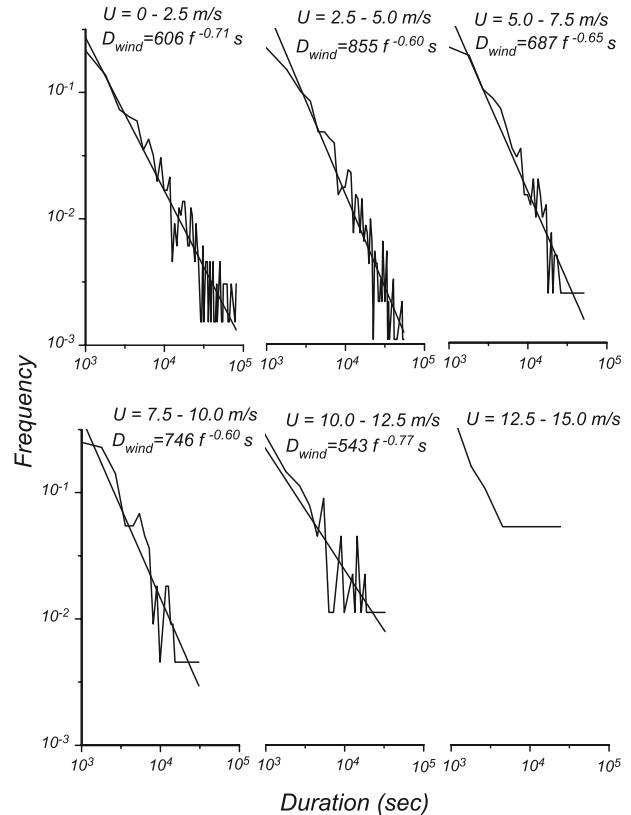

Figure 7. Duration of wind storms for different classes of wind intensity in the Venice lagoon during the period from October 2002 to March 2003.

water column thus increasing the sediment concentration (M is taken as an adjustable parameter in the model and represents different conditions of sediment supply to the tidal flat), f is the fraction of suspended sediment that is lost to the ocean every tidal cycle T (with $T = 12$ h, herein we set $f = 20\%$), u and u_{max} are the instantaneous and maximum tidal velocity during spring tide, respectively. The value of f depends on the redistribution of sediments in the lagoon and the loss through the inlets and can determine, together with the sediment input M, the morphological evolution of the tidal flat. For sake of simplicity, in this preliminary analysis, we decided to maintain f constant and to vary only the sediment input M.

[30] Despite its coarse simplification, this approach captures two important characteristics of sediment dynamics in tidal flats, sediments are imported as a function of tidal fluxes, and tidal flat erosion is due to the resuspension of sediments caused by wind waves and the subsequent export to the ocean. Both sediment deposition and erosion depend on bottom sediment characteristics. Here we differentiate between cohesive and noncohesive sediments.

5.1. Noncohesive Sediments

[31] Limited areas of tidal flats near the three inlets are characterized by very fine sand having an average diameter of 80 μm. For these noncohesive sediments, the erosion rate is set proportional to the excess shear stress, as already used by *Cappucci et al.* [2004] in the Venice lagoon [see also *Fagherazzi and Furbish*, 2001; *Fagherazzi and Sun*, 2003]:

$$\begin{cases} E = 0 & \tau_{tot} \leq \tau_{cr} \\ E = \alpha(\tau_{tot} - \tau_{cr})^{1.5} & \tau_{tot} > \tau_{cr} \end{cases} \quad (15)$$

where α is a rate of erosion whose value, together with the value of critical shear stress, is reported in Table 1.

[32] The deposition rate is instead set proportional to the sediment concentration in the water column:

$$D = rCw_s \quad (16)$$

where w_s is the settling velocity of the sand particles, and r is the ratio between the concentration at the bottom and the average sediment concentration in the water column. Herein we set $r = 1$ as the flow is shallow and the suspended sediment is well mixed in the water column.

5.2. Cohesive sediment

[33] Most of the tidal flats in the Venice lagoon are dominated by clay and silt sediments, with an average grain size of 25 μm [*Amos et al.*, 2004].

[34] For these cohesive sediments, we use the generalized formulation reported in the work of *Sanford and Maa* [2001] to calculate the erosion rate:

$$\frac{dE}{dt} + \beta\gamma E = \beta\frac{d\tau_{tot}}{dt} \quad (17)$$

where β is the rate of erosion equivalent to α in equation (15), and $\gamma = d\tau_{cr} / dz$ is the increase of critical shear stress with depth due to the consolidation of the cohesive sediments (supposed herein locally constant). Equation (17) accounts for the reduction in erosion rates

when the first sediment layer is removed and more resistant layers are exposed to the action of waves and currents. Equation (17) is solved with an explicit finite difference method during each wind event. The erosion rates of both equations (17) and (15) were derived from the literature but not tested in the field.

[35] For the deposition rate, we need to account for the aggregation of sediment flocs at high concentration, and therefore we set the settling velocity proportional to the sediment concentration to the power of 4/3 as determined by *Krone* [1962] in laboratory experiments.

$$D = KC^{7/3}\left[1 - \frac{\tau_{tot}}{\tau_{dep}}\right] \quad (18)$$

where K is reported in Table 1, and $\tau_{dep} = 0.65$ Pa is a critical shear stress for deposition. The term in brackets accounts for a reduction of the deposition rate caused by turbulence when the bottom shear stresses are large.

6. Model Results

[36] The model is applied to three representative locations in the Venice lagoon (Figure 2). The locations were chosen to describe different substrate characteristics and hydrodynamic conditions. The characteristics of each location are reported in Table 1. Location 1 is near the lagoon inlet, and it is characterized by a sandy substrate. Locations 2 and 3 are instead near the basin boundaries and have a bottom composed of clay and silt [*Amos et al.*, 2004].

[37] The temporal evolution of the tidal flat elevation is studied by simulating long-term wind conditions under different scenarios of sediment input and output. At the beginning of the simulation, a value for the sediment-input rate M and sediment loss f are chosen in equation (14). The model simulation procedure consists of nine steps that are repeated every temporal interval: (1) two random numbers $r1$ and $r2$ are drawn from a random uniform distribution defined between 0 and 1 and then used in equation (11) to calculate the wind speed and duration; (2) the tidal elevation and velocity are calculated for the duration of the wind every 30 min from equations (2) and (3); (3) given the wind intensity and the water depth, the wave height is computed from equation (6) for fully developed sea and from equation (8) for fetch limited conditions; (4) given the wave height, the bottom shear stresses are computed from equation (7); (5) the wave shear stresses and the tidal current shear stresses are combined to determine the total shear stress in equation (1); (6) the erosion is calculated from equation (15) for noncohesive and from equation (17) for cohesive sediments; (7) the deposition rate is calculated from equation (16) for noncohesive and from equation (18) for cohesive sediments; (8) the sediment concentration is computed with equations (13) and (14); (9) the bottom elevation is updated in equation (12). A temporal step of 30 min was chosen to resolve in detail the tidal oscillations without compromising computational speed.

[38] An example of model results for location 2 is presented in Figure 8 with $M = 2 \times 10^{-5}$ kg/m^2/s. The temporal series of wind intensity produce waves of elevation up to 0.4 m. Only wind speeds exceeding 3 m/s produce significant waves, and the tidal elevation has a
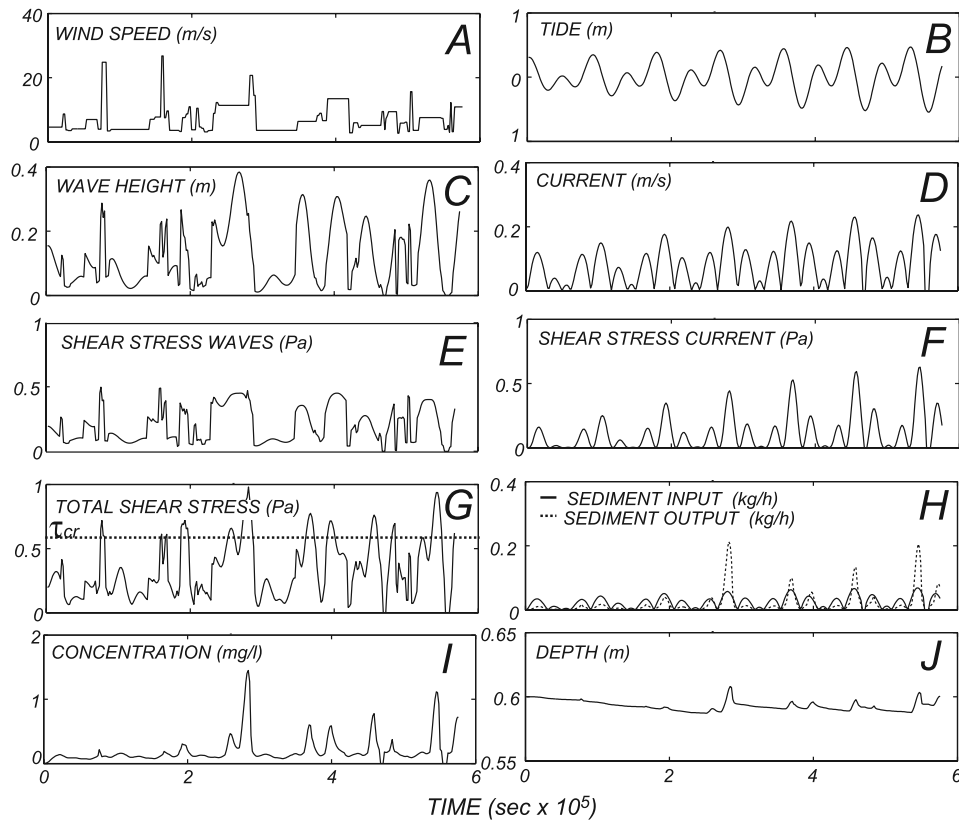
Figure 8. Calculation of bottom shear stresses and elevation as a function of time. (a) Wind velocity as given by the Montecarlo model, (b) tidal level, (c) wave height, (d) tidal current velocity, (e) wave bottom shear stresses, (f) bottom shear stress due to tidal current, (g) total shear stress, (h) sediment input and output at the basin location, (i) sediment concentration, (j) water depth.

marginal effect on modulating the wave height (but the tidal effect becomes important in shallow tidal flats). The wave shear stress is then added to the tidal current shear stresses (Figure 8f) to produce the total shear stress (Figure 8g) responsible for the resuspension of sediments in the water column (Figure 8i) and bottom erosion (Figure 8j). Sediment input (Figure 8h) is on average higher than sediment output during normal wind conditions (small waves), but, when wind waves resuspend a consistent volume of sediments, the tide exports part of this material to the ocean (sediment output, Figure 8h). Superimposition of tidal shear stress to wave shear stress appears to be crucial for bottom erosion. Short wind events of few hours produce erosion when they occur during ebb or flood but are not effective during slack water. Prolonged wind durations spanning at least half a tidal cycle are more effective in eroding the tidal flat bottom, since they are always combined with peak tidal discharges.

[39] Differences in sediment resuspension and bottom evolution for the three locations of Figure 2 are indicated in Figure 9 for the tide and wind conditions shown in Figure 8. The fine sand at location 1 is easily entrained in the water column ($\tau_{cr} = 0.65$ Pa), but the high settling velocity redeposits the sand in a short time interval. As a result, the sediment concentration in the water column experiences sudden increases of short duration related to energetic wind conditions and spring tides. At location 2, the consolidated cohesive material is more difficult to erode

($\tau_{cr} = 0.84$ Pa), and only the combination of waves and currents is able to resuspend the bottom sediments. Since the sediment flocs have a low settling velocity, they remain in suspension for longer periods, so that the sediment concentration is more uniform in time. Erosion occurs only during storm conditions (Figure 9c). A limited fetch reduces the sediment resuspension at location 3. Changes in sediment concentration are clearly dictated by sediment inputs, whereas only extreme wind conditions are able to erode bottom materials. As a consequence, the tidal flat accretes (Figure 9e).

[40] The temporal variation of bottom elevation for different sediment inputs is then studied. Starting with a tidal flat elevation of -1.5 m at location 2, we run the model with different values of the sediment input M ranging from 1×10^{-5} to 4×10^{-5} kg/yr/m^2 (Figure 10). In Figure 10, we also indicate the total annual sediment input, which depends on M and the tidal velocity u. The total annual sediment input can be easily calculated at the end of the simulation by integrating equation (14) without the erosion term and allows comparing the evolution of tidal flats having different hydrodynamic characteristics. Since the total annual sediment input is more significant for intertidal morphodynamics, it will be used throughout the paper in substitution of M.

[41] By analyzing the simulation outcomes in Figure 10, one can see that, after an initial transient period, the tidal flat reaches a dynamic equilibrium elevation at which the
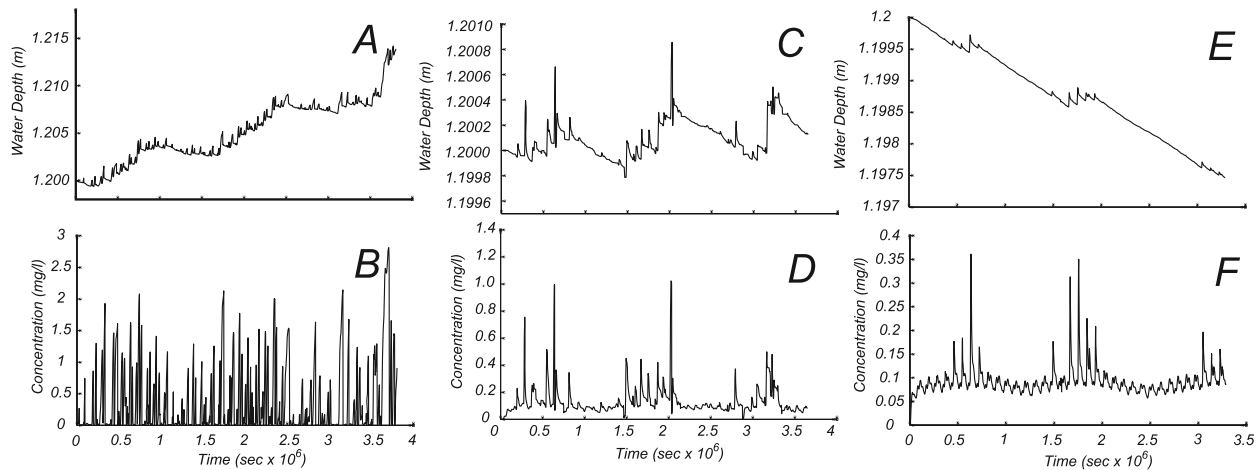
Figure 9. Evolution of water depth and sediment concentration in the water column with the wind field and tidal oscillations of Figure 8. (a) Evolution of the water depth at location 1 and (b) related sediment concentration; (c) water depth and (d) sediment concentration at location 2; (e) water depth and (f) sediment concentration at location 3. All simulations start at a depth of 1.2 m with the same sediment input of Figure 8.

average sediment input and output are equal. The equilibrium elevation strongly depends on the sediment input, as was postulated in the work of *Fagherazzi et al.* [2006]. For increasing sediment inputs, the average tidal flat elevation increases, until the critical elevation (corresponding to the peak in Figure 1) is reached. Then, as expected, for higher inputs the tidal flat becomes a salt marsh. By plotting the equilibrium elevation as a function of the sediment input for the three tidal flats, we note that the elevation increases until a critical point above which the tidal flat becomes unstable (Figure 11). In the two tidal flats with unlimited fetch, the critical depth is around −1.4 m, despite differences in substrate composition. At location 3, where the fetch is on average 1000 m, the critical elevation is −0.5 m, since the peak in shear stress shifts toward shallower depths (see Figure 5). These preliminary results confirm that the critical elevation above which the tidal flat becomes unstable strongly depends on fetch conditions. Sediment characteristics (cfr. locations 1 and 2) do not affect the critical elevation but determine the sediment input necessary to move the tidal flat in the range of unstable elevations. In fact, for sandy bottoms, the sediment input has to be five times larger in order to destabilize the tidal flat. In fetch limited conditions lower sediment inputs are sufficient to trigger a transition toward marsh elevations, since the small waves are unable to resuspend bottom sediments. The transition from tidal flat to salt marsh depends on the statistical properties of the wind. Long periods of calm wind conditions can favor deposition and the transition from tidal flats to salt marshes, whereas an intense storm can transform an incipient salt marsh in a tidal flat, so that flats having an elevation around the peak in shear stress can reverse their evolution trend.

[42] Near the critical elevation, the oscillations in bottom elevation are greater (Figure 10), since erosion is magnified by large wave heights (we are near the peak in shear stress of Figure 1). Under these conditions, the system is highly dynamic, with each storm having a strong impact on the tidal flat elevation. Our model results clearly indicate that

tidal flats experiencing strong variations in elevation in time are near critical conditions, and they can easily morph into a salt marsh in few years (Figure 10). The curves in Figure 5 were derived by *Fagherazzi et al.* [2006] with only one, geomorphologically significant wind intensity, whereas in natural conditions tidal flats are subject to a series of wind events of different intensity and duration. This notwithstanding, it is remarkable how the critical depths that separates the stable from the unstable component in Figure 11 are very close to the peak values in Figure 5.

7. Influence of Tidal Oscillations on the Dynamic Equilibrium of Tidal Flats

[43] In the conceptual model of *Fagherazzi et al.* [2006], a geomorphically significant wind speed [e.g., *Wolman and*
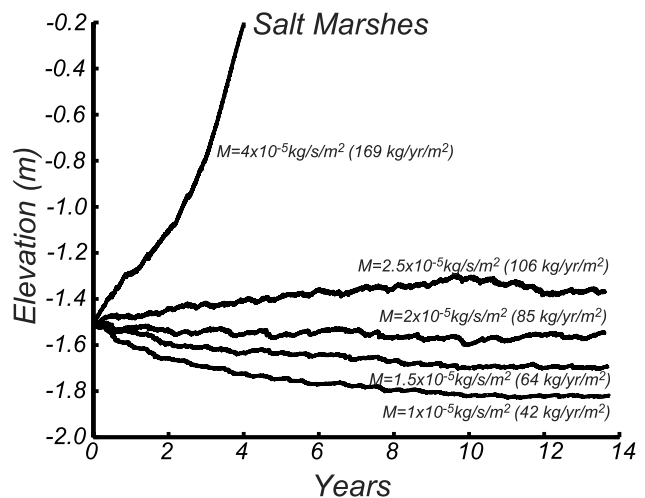

Figure 10. Tidal flat elevation as a function of time for different sediment inputs. All simulations start from −1.5 m below m.s.l. For input rates higher than 2.5×10^{-5}kg/s/m^2, the tidal flat becomes a salt marsh.
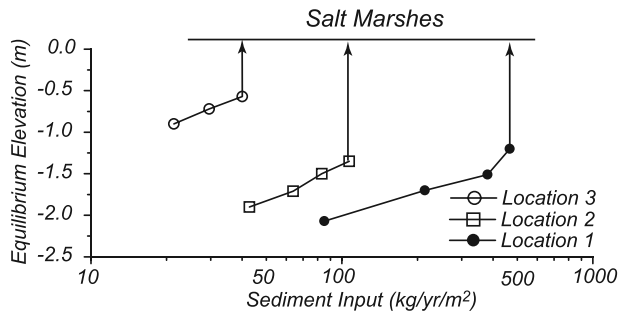
Figure 11. Tidal flat equilibrium elevation as a function of sediment input for the three tidal flats of Figure 2. For an unlimited fetch, elevations below −1.4 m become unstable, whereas for a fetch of 1000 m, the critical elevation is −0.5 m. The equilibrium elevation was calculated after a simulation of 20 years.

Figure 13. Comparison between two simulations with and without tide and a sediment input rate of 42 kg/yr/m². The simulations start at 1.5 m above m.s.l. In the simulation without tides, the tidal flat is unable to attain an equilibrium elevation and will therefore emerge.

Miller, 1960] was used to derive the distribution of shear stresses as a function of tidal flat depth (Figures 1 and 5). In reality, the local distribution of wind intensity and duration determines the elevation of tidal flats, whereas tidal oscillations have a key role in modulating bottom shear stresses. As a consequence, the functional dependence between shear stress and elevations can be more complex than the one reported in Figures 1 and 5. To verify the validity of the assumptions utilized for Figure 1, we plot in Figure 12 the distribution of bottom shear stress as a function of elevation for a simulation with tides and observed wind characteristics. We choose a sediment input of 200 kg/yr/m² that is large enough to lead to the formation of a salt marsh and we start at an elevation of −2.0 m at location 2. During the slow accretion, the tidal flat experiences a series of random storms with characteristics similar to the ones observed in the Venice lagoon. If the accretion is slow enough, for each tidal flat elevation, we sample all the possible shear stresses acting on the lagoon bottom. The envelop of these stresses is then the maximum possible shear stress acting on the tidal flats as a function of elevation. As it can be seen in Figure 12, the distribution of shear stresses mimics Figure 1 with a peak at a depth close to 1.0 m. Of interest
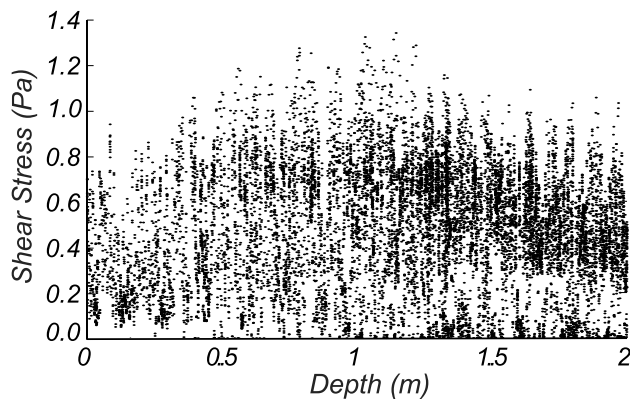
are also the monthly patterns in shear stress that emerge from Figure 12, indicating that the spring-neap modulation is critical for the distribution of shear stress.

[44] Our modeling approach allows studying the separate influence of tidal oscillations on the equilibrium elevation of tidal flats and its variance in time. Tidal oscillations have two important effects on bottom erosion, they modulate water depths and produce oscillatory currents that enhance bottom shear stresses. To separately determine the role of tidal oscillations, we compare our results to a simulation in which the ocean level is maintained fixed (Figure 13). Instead of eliminating tidal currents, which would inevitably reduce bottom shear stresses, we use a constant value of $u = 0.058$ m/s obtained by averaging the absolute value of the velocity in equation (2). By doing so, the average water depth and current velocity are the same in both cases, with and without tide, and the elevation differences of the flat stem from the nonlinear effects of the oscillations of these quantities on erosion rates. Tidal oscillations can have a twofold effect on sediment erosion. At low tide, the water depth is reduced so that the shear stresses are enhanced at the bottom, whereas at high tide, wave driven erosion is limited since the bottom is too far to feel the waves. Furthermore, the concentration of tidal fluxes during spring tide can increase the overall erosion and thus become critical for tidal flat evolution. In our simulation at location 2 without tides, even with a low sediment input rate of 42 kg/yr/m², the tidal flat accretes toward an elevation range typical of salt marshes. This indicates that the spring-neap modulation of tidal velocity is critical for tidal flat equilibrium.

8. Conclusions

[45] Simulations of tidal flat evolution carried out with a simple stochastic point model for wind waves sediment resuspension show that the transition from tidal flats to salt marshes is not a continuous process but occurs abruptly when the sediment input at the specific basin location reaches a critical value related to the local wind climate and fetch length.

[46] Given a specific sediment input below the critical value, wind driven sediment resuspension maintains the

Figure 12. Distribution of shear stresses as a function of tidal flat elevation. The distribution was obtained with a sediment input of 1700 kg/s/m² starting from a bottom depth of 2 m. The sediment input rate is large enough to create a salt marsh at the end of the simulation.
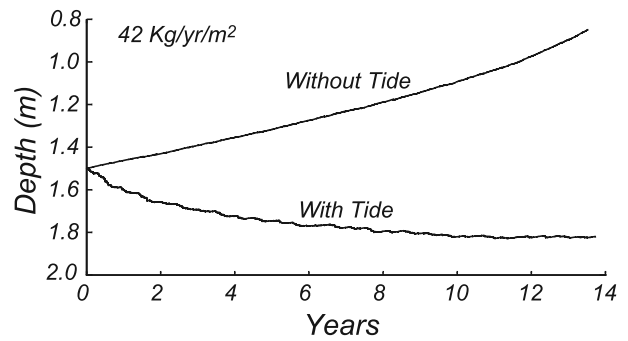
tidal flat below mean sea level. The equilibrium elevation depends on the relationship between shear stress caused by wind waves and depth. It is found that wind wave shear stresses peak for a specific water depth which is a function of the local wind and wave climate and fetch distance. Above this depth, tidal flats are unstable, since an increase in elevation reduces wave height and therefore erosion, preventing the system from recovering equilibrium conditions.

[47] Given the wave climate of the Venice lagoon, for locations having unlimited fetch, the unstable range of elevations starts at −1.5 m, whereas for locations with a fetch of 1000 m, the critical elevation is at −0.6 m. This difference explains why in the southern part of the Venice Lagoon, whose water surface is open, the tidal flats are on average at elevations between −1.5 and −2.5 m, whereas in the Northern Lagoon, where islands and salt marshes considerably limit the fetch distance, the average tidal flat elevation is between −0.4 and −1.0 m (Figure 2).

[48] The critical equilibrium elevation is independent of substrate characteristics. Instead, the substrate determines the sediment input necessary to maintain the tidal flat in equilibrium. Given a tidal flat elevation, the sediment input necessary to maintain a tidal flat with a fine sand substrate in dynamic equilibrium is five times higher than the one required for a tidal flat with cohesive sediments. Similarly, at locations with limited fetch, the sediment input necessary for equilibrium is much lower, since the reduced wind waves limit tidal flat erosion.

[49] Tidal flats with an equilibrium elevation close to the peak in shear stress have depths that vary in time, since each storm has a high impact on bottom sediments. Therefore a high variability in tidal flat elevation is a possible signal of instability and incipient transformation to salt marsh.

[50] Bottom shear stresses are modulated by tidal oscillations, with higher stresses during spring tides. Our results indicate that peak velocities during spring tide superimposed to wind waves are critical for tidal flat equilibrium, whereas in the absence of spring-neap modulation, tidal flat elevations below mean sea level could not be maintained.

[51] The elevations of the three tidal flats used as examples herein agree with these findings. Locations 1 and 2 have an elevation of −2.0 and −2.4 m, respectively (see Table 1), well below the critical value of −1.5 m. Therefore these tidal flats are far from the unstable range of elevations and an increase in sediment input will just produce a shoaling and the attainment of a new equilibrium depth. Location 3 has an elevation of −0.6 m, very close to the critical equilibrium elevation calculated by our model. Therefore an increase in sediment availability in this area could destabilize the tidal flat and trigger the formation of a salt marsh.

[52] In our analysis, we have neglected the feedbacks between wind stresses and tidal circulation that can have important consequences for intertidal morphodynamics. In fact, tidal patterns change significantly when the wind blows inland or offshore. Wind direction, which was not included in the model, can also have a strong influence on fetch length, resuspension, and sediment patterns in intertidal areas. We have also neglected the possible presence of biofilms on the sediment surface during summer months. These biofilms increase the resistance to erosion as indicated by the preliminary data of *Amos et al.* [2004]. Future

research will focus on these aspects of sediment transport. The same framework can be utilized in coastal environments (for example, tidal basins, bays, and estuaries) where the distribution of wind wave shear stresses peaks for an intermediate depth and tidal oscillations modulate the flow velocity. All these results are limited to mesotidal and microtidal flats, where the chief geomorphic agent for sediment resuspension are wind driven waves. In areas where the tidal excursion is high, tidal fluxes and their spatial variability shape the landscape and control the dynamic equilibrium of the tidal flats.

References

Allen, J. R. L. (1990), Salt-marsh growth and stratification: A numerical model with special reference to the Severn Estuary, southwest Britain, *Mar. Geol.*, *95*(2), 77−96.

Allen, J. R. L. (1995), Salt-marsh growth and fluctuating sea level: Implications of a simulation model for Flandrian coastal stratigraphy and peat-based sea-level curves, *Sediment. Geol.*, *100*(1−4), 21−45.

Allen, J. R. L., and M. J. Duffy (1998), Medium-term sedimentation Medium-term on high intertidal mudflats and salt marshes in the Severn Estuary, SW Britain: The role of wind and tide, *Mar. Geol.*, *150*(1−4), 1−27.

Amos, C. L., A. Bergamasco, G. Umgiesser, S. Cappucci, D. Cloutier, L. DeNat, M. Flindt, M. Bonardi, and S. Cristante (2004), The stability of tidal flats in Venice Lagoon—The results of in-situ measurements using two benthic, annular flumes, *J. Mar. Syst.*, *51*(1−4), 211−241.

Booij, N., R. C. Ris, and L. H. Holthuijsen (1999), A third-generation wave model for coastal regions-1. Model description and validation, *J. Geophys. Res.*, *104*(C4), 7649−7666.

Cappucci, S., C. L. Amos, T. Hosoe, and G. Umgiesser (2004), SLIM: A numerical model to evaluate the factors controlling the evolution of intertidal mudflats in Venice Lagoon, Italy, *J. Mar. Syst.*, *51*(1−4), 257−280.

Carniello, L., A. Defina, S. Fagherazzi, and L. D'Alpaos (2005), A combined wind wave−tidal model for the Venice lagoon, Italy, *J. Geophys. Res.*, *110*(F4), F04007, doi:10.1029/2004JF000232.

D'Alpaos, A., S. Lanzoni, S. M. Mudd, and S. Fagherazzi (2006), Modeling the influence of hydroperiod and vegetation on the cross-sectional formation of tidal channels, *Estuarine Coastal Shelf Sci.*, *69*(3−4), 311−324.

Defina, A. (2000), Two dimensional shallow flow equations for partially dry areas, *Water Resour. Res.*, *36*(11), 3251−3264.

Exner, F. M. (1925), Uber die Wechselwirkung zwischen Wasser und Geschiebe in Flussen, *Sitzber. Akad. Wiss Wien, Part IIa*, 134.

Fagherazzi, S., and T. Sun (2004), A stochastic model for the formation of channel networks in tidal marshes, *Geophys. Res. Lett.*, *31*(21), L21503, doi:10.1029/2004GL020965.

Fagherazzi, S., and D. J. Furbish (2001), On the shape and widening of salt marsh creeks, *J. Geophys. Res.*, *106*, 991−1005.

Fagherazzi, S., A. Bortoluzzi, W. E. Dietrich, A. Adami, S. Lanzoni, M. Marani, and A. Rinaldo (1999), Tidal networks: 1. Automatic network extraction and preliminary scaling features from digital elevation maps, *Water Resour. Res.*, *35*(12), 3891−3904.

Fagherazzi, S., P. L. Wiberg, and A. D. Howard (2003), Tidal flow field in a small basin, *J. Geophys. Res.*, *108*(C3), 3071, doi:10.1029/2002JC001340.

Fagherazzi, S., L. Carniello, L. D'Alpaos, and A. Defina (2006), Critical bifurcation of shallow microtidal landforms in tidal flats and salt marshes, *Proceedings of the National Academy of Sciences of the United States of America*, *103*(22), 8337−8341.

French, J. R. (1993), Numerical simulation of vertical marsh growth and adjustment to accelerated sea-level rise, North Norfolk, UK, *Earth Surf. Processes Landforms*, *18*(1), 63−81.

Gardner, L. R. (2004), Geologic history and the ergodic principle: Foundations for long-term ecological research in salt marshes, in *The Ecogeomorphology of Salt Marshes, Estuarine and Coastal Studies Series*,

edited by S. Fagherazzi, M. Marani, and L. K. Blum, pp. 189–201, American Geophysical Union, Washington, D. C.

Krone, R. B. (1962), Flume studies of the transport of sediment in estuarial shoaling processes, University of California, Berkeley, Hydraulics Engineering Laboratory and Saint Engineering Laboratory.

Krone, R. B. (1987), A method for simulating historic marsh elevations, in *Coastal Sediments '87*, edited by N. C Krause, pp. 316–323, American Society of Civil Engineers, New York.

Marani, M., E. Belluco, A. D'Alpaos, A. Defina, S. Lanzoni, and A. Rinaldo (2003), On the drainage density of tidal networks, *Water Resour. Res.*, *39*(2), 1040, doi:10.1029/2001WR001051.

Morris, J. T., P. V. Sundareshwar, C. T. Nietch, B. Kjerfve, and D. R. Cahoon (2002), Responses of coastal wetlands to rising sea level, *Ecology*, *83*, 2869–2877.

Mudd, S. M., S. Fagherazzi, J. T. Morris, and D. J. Furbish (2004), Flow, sedimentation, and biomass production on a vegetated salt marsh in south carolina: toward a predictive model of marsh morphologic and ecologic evolution, in *The Ecogeomorphology of Tidal Marshes*, edited by S. Fagherazzi, M. Marani, and L. K. Blum, vol. 59, 266 p., American Geophysical Union Coastal and Estuarine Studies, Washington, D. C.

Pethick, J. S. (1981), Long-term accretionrates on tidal slat marshes, *J. Sediment. Petrol.*, *51*(2), 571–577.

Rinaldo, A., S. Fagherazzi, S. Lanzoni, M. Marani, and W. E. Dietrich (1999a), Tidal networks 2. Watershed delineation and comparative network morphology, *Water Resour. Res.*, *35*(12), 3905–3917.

Rinaldo, A., S. Fagherazzi, S. Lanzoni, M. Marani, and W. E. Dietrich (1999b), Tidal networks 3. Landscape-forming discharges and studies in empirical geomorphic relationships, *Water Resour. Res.*, *35*(12), 3919–3929.

Sanford, L. P., and J. P. Y. Maa (2001), A unified erosion formulation for fine sediments, *Mar. Geol.*, (1–2), 9–23.

Sheng, Y. P., and W. Lick (1979), The transport and resuspension of sediments in a shallow lake, *J. Geophys. Res.*, *84*, 1809–1826, 1979.

Silvestri, S., A. Defina, and M. Marani (2005), Tidal regime, salinity and salt marsh plant zonation, *Estuarine Coastal Shelf Sci.*, *62*, 119–130, doi:10.1016/j.ecss.2004.08.010.

Soulsby, R. L. (1997), *Dynamics of Marine Sands: A Manual for Practical Applications,* 248 pp., Thomas Telford, London.

Temmerman, S., G. Govers, P. Meire, and S. Wartel (2004a), Simulating the long-term development of levee-basin topography on tidal marshes, *Geomorphology*, *63*(1–2), 39–55.

Temmerman, S., G. Govers, S. Wartel, and P. Meire (2004b), Modelling estuarine variations in tidal marsh sedimentation: Response to changing sea level and suspended sediment concentrations, *Mar. Geol.*, *212*(1–4), 1–19.

Wolman, M. G., and J. P. Miller (1960), Magnitude and frequency of forces in geomorphic processes, *J. Geol*, *68*, 54–74.

————————————

L. Carniello and A. Defina, Department IMAGE, University of Padova Via Loredan, 20, 35131 Padua, Italy.

S. Fagherazzi, Department of Earth Sciences and Center for Computational Science, Boston University, Boston, MA 02215, USA. (sergio@bu.edu)

C. Palermo and M. C. Rulli, Department of Hydraulic, Environmental, Road and Surveying Engineering Hydraulics, Politecnico di Milano, 20133 Milan, Italy.